applied sciences

MDPI

Article

The Combined Magneto Hydrodynamic and Electric Field Effect on an Unsteady Maxwell Nanofluid Flow over a Stretching Surface under the Influence of Variable Heat and Thermal Radiation

Hameed Khan [1], Muhammad Haneef [1], Zahir Shah [2,*], Saeed Islam [2], Waris Khan [3] and Sher Muhammad [3]

1 Lab of Theoretical Physics, Department of Physics, Hazara University, Mansehra 21300, KP, Pakistan; danyalhameed2009@gmail.com (H.K.); haneef.theoretician@gamil.com (M.H.)
2 Department of Mathematics, Abdul Wali Khan University, Mardan 23200, KP, Pakistan; proud_pak@hotmail.com
3 Department of Mathematics, Islamia College, Peshawar 25000, KP, Pakistan; wariskhan758@yahoo.com (W.K.); shermphil123@gmail.com (S.M.)
* Correspondence: zahir1987@yahoo.com; Tel.: +92-333-9198-823

Received: 10 December 2017; Accepted: 17 January 2018; Published: 24 January 2018

Abstract: The manuscript is a presentation of the combined effect of magnetic and electric field on unsteady flow of Maxwell nanofluid over a stretching surface with thermal radiations. The flow of Maxwell nanofluid is assumed to be in an unsteady state. The basic governing equations changed to a group of differential equations, using proper similarity variables. The obtained modeled equations are nonlinear and coupled. An optimal approach is used to acquire the solution of the modeled problem analytically. The effects of electric field, magnetic field and thermal radiations on Maxwell nanofluid are the main focus in this study. The impact of the Skin friction on velocity profile, Nusselt number on temperature profile and Sherwood number on concentration profile are studied numerically. The influential behavior of the unsteady parameter λ, magnetic parameter M, electric parameter E, radiation parameter Rd, Maxwell parameter β, thermophoresis parameter Nt, Prandtl number Pr, Schmidt number Sc, space dependent coefficient A and temperature dependent coefficient B on the velocity $f(h)$, concentration $\phi(\eta)$ and temperature $\theta(\eta)$ are analyzed and studied. The consequences are drawn graphically to see the physical significance of the problem.

Keywords: nanofluid; unsteady flow; stretching sheet; thermal radiations; electric field; magnetic field; HAM

1. Introduction

Two-dimensional boundary layer flow problems of nanofluid flow, heat and mass transmission over a stretched heated surface with magnatohydrodynamic effects have an abundant and extensive range of applications in various engineering and industrial disciplines. These include glass blowing, extrusion process, melt-spinning, design of heat exchangers, wire and fiber coating, glass fiber production, manufacturing of plastic and rubber sheets, etc. Magneto hydrodynamics is the knowledge of magnetic assets of electrically conducting fluids. Plasmas, salt water, electrolytes and liquid metals are examples of such magneto fluids. Alfven [1] pioneered the field of Magnetohydrodynamic (MHD). Magnetohydrodynamics have numerous practical usages in the field of engineering and technology, such as crystal growth, liquid-metal cooling of reactors, plasma, magnetohydrodynamic sensors, electromagnetic casting, MHD power generation and magnetic drug targeting. Magnetohydrodynamic depend upon the strength of the magnetic inductions.

Eccentric features of nanofluids make them proficient in various applications. Nanofluids are used in pharmaceutical procedures, hybrid powered engines, fuel cells, microelectronics and currently, they are vastly used in the field of nanotechnology. Maxwell fluids is the most important subclass of non-Newtonian fluids, and are commonly used in industries and technology of paints, paper pulps, drilling muds, shampoos, certain oils and polymer solutions, which have a nature of Maxwell fluid [2]. Several researchers investigated Maxwell fluid with the effect of heat and MHD. Few data are available on it in the form of Nanofluids. Researchers have shown great interest in the Maxwell fluid, owing to its physical importance. It has numerous applications in various fields of engineering and industry and in some other disciplines of technologies. Melting, spinning, design of heat exchangers, fiber coating, manufacturing of plastics sheet, food stuff, vehicle's engine, Nano chips and the extradition from the dye are some of the important applications of Maxwell fluids, while nanofluids have different applications, for example engine cooling, defense, improving efficiency of diesel generator and cooling of electronic appliances [3]. Nanoparticles include metals, carbons, metal oxides and inorganic materials. They have no dissolution properties of the base fluid. Experimental investigations [4–8] reveal that adding metals or metallic oxides to the base fluid increases thermal conductivity which results in increase of heat transfer rates. The main concept behind nanoparticles is the transfer of heat easily.

The electric field has a great role in fluid dynamics [9]. To improve the rate of heat transfer in fluids, different authors have worked from different angles. The role of electrodes is important in heat transfer, which is studied by Kasayapan. The influence of electric field on a plate in fluid flow is studied by Godfreg et al. [10]. Yan et al. [11] have found that applying a non-uniform electric field has better results than uniform electric field. Electro-kinetic is also one of the important methods of flow, which enhance the fluid flow. In electro-kinetic, an electric potential is applied across the micro-channel. The applied electric potential is not so high in magnitude because the electrical layer EDL is much smaller than the micro-channel. The electrically motivated flow with pressure is much better than the driven pressure, flow because it reduces device scale. Some of the articles on electro-kinetic method of flow in different systems is presented in [12]. The electric field has also important applications in medical sciences. The micro fluid under electro-kinetic delivers drugs quickly with low power in self-ruling microsystem. The electro-kinetic influences on nanoparticles are important because a non-uniform field applies to the suspension that exerts force on the nanoparticles. The high power field produces an extra force on the suspension as well as on the medium. Influence on viscosity of nanofluid due to electric field are studied by Monajjemi et al. [13]. They concluded that the diluted solution of ethylene glycol viscosity decreases with applying a voltage and especially DC voltage reduces viscosity of the fluid more rapidly.

The effect of radiations on fluid flow and its application was started by Plum [14]. The radiated phenomena in fluid flow have vital importance in industry. It is used for various purposes, such as in design of nuclear plants, fire propagation [15], plume dynamics [16], materials processing [17], rocket propulsion [18], and missiles, aircraft and space technology. Mansour et al. [19] studied the thermal radiation effect on magnetic hydrodynamic fluid flow. Thermal radiations play a vital role in monitoring the heat relocation in the polymer preparation industry. The class of the final product can be determined to a great extent by knowledge of radiated heat transfer and heat controlling factors in the system, which can lead to a preferred creation with required qualities. The efficiency of common fluid in thermal systems is lower compared to a fluid that consists of nanoparticles because it improves the suspension features [20]. The efficiency of common base fluid for thermal system is comparatively poor. Mostly non-Newtonian fluids are used in industry as compared to Newtonian fluids. The relationship between stress and strain is linear in a Newtonian fluid, while, in non-Newtonian fluids, this relation is nonlinear [21]. To improve heat transfer, the thermophysical character of the base fluid is studied. The addition of nanoparticle (metal) to the base fluid improves thermal characteristic which enhances the heat transfer of a fluid. Khanaferet et al. [22] have investigated and found that the addition of nanoparticles enhances Nusselt Number. Nanofluid investigated by other researchers as well

and different methods have been used by them to improve their features [23–28]. Confinement of channel enhances the thermal conductivity of the nanofluid [29]. The nanofluid flow in narrow channels enhances the thermal conductivity by approximately 20% [30]. Papanikolaou et al. [31] investigated the effect of roughness of the surface on nanofluid flow. Stretching into a uniform sheet is a phenomenon in which sheets become unidirectional, which gives a good characteristic to polymers sheet manufacturing. Different kinds of sheets are prepared in industry, including stretching sheets. Stretching sheets can transfer mass and heat immediately and are presently used in different areas. Steady two-dimensional fluid flows were studied by Sikiadis et al. [32]. Crane et al. [33] expanded the problem for varying velocity with a fixed point. Gupta et al. [34] studied steady fluid in the presence of stretching surface considering suction. Later, Grubka et al. [35] studied heat relocation over a stretching surface through variable temperature. In all the previous investigations, steady flow has been discussed. For more realistic physical applications, unsteadiness has been introduced to the flow. Wang et al. [36] investigated unsteadiness for the first time. Bazed et al. [37] added heat to the unsteady flow over a stretching surface. Chamka et al. [38,39] studied three-dimensional unsteady flows. To the best of the author's knowledge, the combined effect of electric and magnetic fields on unsteady stretching flow with thermal radiations has not been investigated yet. It has a wide range of applications such as in nuclear reactors, magnetic hydrodynamic generators and polymers extrusion.

In 1992, Liao [40–42], for the first time, examined this method for the solution of nonlinear problems and proved that this method is quickly convergent to the approximated solutions. In addition, this technique provides series solutions in the form of functions of a single variable. Solution with this method is important because it involves all the physical parameters of the problem and we can simply discuss its behavior.

The main aim of this work is to investigate the effect of electric field, magnetic field and thermal radiation on the mentioned fluid. The problem is solved analytically. Different methods of simulations are used in the literature [43–45], e.g., molecular dynamic (MD) simulation, computational fluid dynamic (CFD) simulations, hybrid CFD-MD and MD (CGMD) simulation. Each method is used for different state. CFD is used for continuum simulation. Hybrid simulations such as MD (CGMD) are applicable to solids, where atoms are relatively fixed with respect to each other. Each simulation has good analytical results in the respective state such as macroscopic dynamic, microscopic dynamic, fluid, solid and gases. For the current purpose, the basic governing equations are changed to a group of differential equations, and further Homotopy Analysis Method (HAM) is used to acquire the solution of the modeled problem analytically. The embedded physical parameters are drawn graphically and discussed in detail.

2. Formulation of the Problem

Consider the two-dimensional time dependent and thermally and electrically conducting flow of Maxwell nanofluid moving on the vertical continuous stretching sheet which passes through a thin slot. The flow is along y-direction which is shown schematically in Figure 1. The uniform magnetic field B_0 and electric field E_0 are applied to the thermal extrusion forming stretching sheet along the y-direction. The concentration C_w and temperature T_w of the nanoparticles are kept uniform where these values are supposed to be greater than ambient concentration and temperature. The fluid flow is considered to be limited in a region where $y > 0$. The internal heat is taken to be non-uniform in absorption/generation to know the concentration and temperature variances between the fluid and the surfaces. The velocity is expected to be directly proportional to the space taken from the slit.

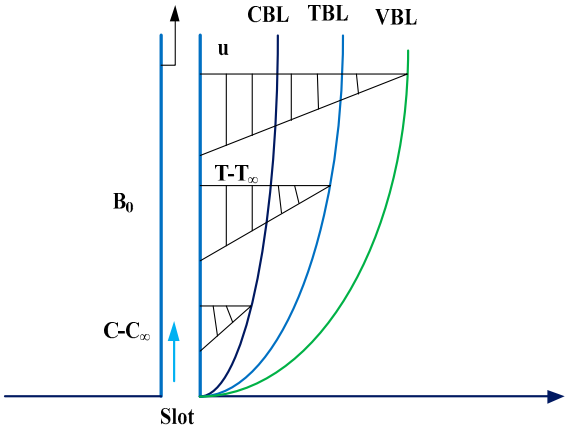

Figure 1. The schematic diagram of the Maxwell nanofluid flow.

The governing equation of energy, mass and momentum in existence of magnetic field and heat source is expressed as Equations (1)–(3).

$$div\vec{V} = 0, \tag{1}$$

$$\rho\frac{d\vec{V}}{dt} = divT + \vec{J} \times \vec{B}, \tag{2}$$

$$(\rho c)_p \frac{DT}{Dt} = T.\frac{\delta\vec{V}}{\delta x} + K\frac{\partial^2 T}{\partial t^2} + Q(T - T_\infty). \tag{3}$$

where $\vec{B}$ denotes the magnetic field in the direction of y-axis, $\vec{J}$ is the current density and defined as $\vec{J} = \sigma(\vec{V} \times \vec{B})$, k is thermal conductivity and represents specific heat, σ is electrical conductivity, and $\vec{V}$ is fluid velocity where $\vec{V} = \{u(x,y), v(x,y), 0\}$. Here, $\vec{J} \times \vec{B}$ is the Lorentz force and it is reduced to the form of $\vec{J} \times \vec{B} = -\sigma\vec{B_0}^2\vec{V}$. The flow of the nanofluid and heat transfer is assumed in unsteady state which is incompressible, laminar and stable. Keeping in view the above deliberation, the basic equations of continuity, velocity, energy and concentration are reduced as:

$$\frac{\partial\vec{u}}{\partial x} + \frac{\partial\vec{v}}{\partial y} = 0, \tag{4}$$

$$\frac{\partial\vec{u}}{\partial t} + \vec{u}\frac{\partial\vec{u}}{\partial x} + \vec{v}\frac{\partial\vec{u}}{\partial y} + \lambda\left(\vec{u}^2\frac{\partial^2\vec{u}}{\partial x^2} + \vec{v}^2\frac{\partial^2\vec{u}}{\partial x^2} + 2\vec{u}\vec{v}\frac{\partial^2\vec{u}}{\partial x\partial y}\right) = \nu\frac{\partial^2\vec{u}}{\partial y^2} - \frac{\sigma\vec{B}_0^2}{\rho_f}\vec{u} - \frac{\sigma\vec{B}_0\vec{E}_0}{\rho_f}, \tag{5}$$

$$\frac{\partial T}{\partial t} + \vec{u}\frac{\partial T}{\partial x} + \vec{v}\frac{\partial T}{\partial y} = \frac{k}{\rho c_p}\frac{\partial^2 T}{\partial y^2} - \frac{1}{\rho c_p}\frac{\partial q_r}{\partial y} + \frac{1}{\rho c_p}(q'''), \tag{6}$$

$$\frac{\partial C}{\partial t} + \vec{u}\frac{\partial C}{\partial x} + \vec{v}\frac{\partial C}{\partial y} = D_m\frac{\partial^2 C}{\partial y^2} - \frac{\partial}{\partial y}\left(\vec{V}_T C\right), \tag{7}$$

The relevant boundary conditions are:

$$\begin{aligned} &\vec{u} = \vec{U}_w(x,t),\ \ \vec{v} = \vec{V}_w,\ \ T = T_w(x,t),\ \ C = C_w(x,t),\ \ at\ \ y = 0, \\ &\vec{u} \to 0,\ \ T \to T_\infty,\ \ C \to C_\infty,\ \ \text{at}\ \ y \to \infty. \end{aligned} \tag{8}$$

where $\vec{v}$ and $\vec{u}$ are components of velocity along $\vec{y}$ and $\vec{x}$ directions, respectively, t is the time, $\vec{U}_w(x,t)$ is the stretching sheet velocity, $T_w(x,t)$ is the stretching surface temperature, $C_w(x,t)$ represents the concentration of the stretching surface, T_∞ represents the temperature, which is far from the extending surface with $T_w > T_\infty$ and C_∞ is the representation of concentration which is far away from the

extending surface with $C_w > C_\infty$. The term $\overrightarrow{V}_w = -\sqrt{\frac{v\overrightarrow{U_w}}{2x}}f(0)$ shows the mass transmission at the surface with $\overrightarrow{V}_w < 0$ for suction and $\overrightarrow{V}_w > 0$ for injection. The source/sink is non-uniform term q''', defined as:

$$q''' = \frac{\kappa U_w(x,t)}{xv}\big(A(T_w - T_\infty)f' + (T - T_\infty)B\big), \tag{9}$$

where A and B represent temperature- and space-dependent coefficients. When A and B greater than zero, they link to inner heat source, and, when A and B are less than zero, they correspond to inner heat sink. The sheet is stretched, thus flow of nanofluid is caused, and it moves with the surface velocity, temperature and concentration in the form

$$\overrightarrow{U}_w(x,t) = \frac{ax}{1-ct}, T_w(x,t) = T_\infty + \frac{ax}{1-ct}, C_w(x,t) = C_\infty + \frac{ax}{1-ct}, \tag{10}$$

where c and a represents stretching parameter respectively, which are positive constants with $ct < 1, c \geq 0$. It is perceived that the extending rate $\frac{a}{1-ct}$ is increases with time t since $a > 0$. The similarity variables are presented as

$$\eta = \sqrt{\frac{a}{v(1-ct)}}y, \overrightarrow{u} = \frac{ax}{1-ct}f'(\eta), \overrightarrow{v} = -\sqrt{\frac{va}{1-ct}}f(\eta), \theta(\eta) = \frac{T - T_\infty}{T_w - T_\infty}, \ \phi(\eta) = \frac{C - C_\infty}{C_w - C_\infty}. \tag{11}$$

In Equation (6), applying the Rosseland approximation for thermal radiation, the heat flux q_r is demarcated as $q_r = -\frac{4\sigma^*}{3K^*}\frac{\partial T^4}{\partial y}$, where σ^* is called the of Stefan–Boltzmann constant and K^* is known as the mean absorption coefficient. The temperature differences are such that the term T^4 within the flow is a function of the temperature. Using Taylor series, T^4 takes the form of free watercourse temperature T_∞:

$$T^4 = T_\infty^4 + 4T_\infty^3(T - T_\infty) + 6T_\infty^2(T - T_\infty)^2 + ..., \tag{12}$$

Ignoring those terms exhibiting higher-order and beyond $(T - T_\infty)$, the obtain result is

$$T^4 \cong 4T_\infty^3 T - 3T_\infty^4, \tag{13}$$

Thus, adding Equation (13), q_r reduce to the form of

$$q_r = -\frac{16T_\infty^3\sigma^*}{3K^*}\frac{\partial^2 T}{\partial y^2}, \tag{14}$$

The thermophoresis influence is discussed with the help of average velocity attained by minute particles as compared to gas particles, where temperature variations is brought. In the flow, the temperature variations in x-direction is less than in y-direction, which is why only the V_T along y-axis is considered. Thus, the velocity of thermophoretic V_T, as seens in Equation (10), is articulated as:

$$\overrightarrow{V}_T = -\frac{k_1 v}{T_R}\frac{\partial T}{\partial y}, \tag{15}$$

in which T_R is the reference temperature coefficient. Using Equation (11), Equations (7)–(13) take the form of

$$f''' + ff'' - f'^2 - \lambda\Big(f' + \frac{\eta}{2}f''\Big) - \beta\Big(f'^2 f''' - 2ff'f'''\Big) - Mf' - MEI = 0, \tag{16}$$

$$(1 + \frac{4}{3}Rd)\theta'' + \Pr\Big[\big(f\theta' - f'\theta\big) - \lambda\Big(\theta + \frac{\eta}{2}\theta'\Big)\Big] + \big(Af' + B\theta\big) = 0, \tag{17}$$

$$\phi'' + Sc\Big[f\phi' - f'\phi - \lambda\Big(3\phi + \frac{\eta}{2}\phi'\Big)\Big] - Nt\big(\theta'\phi' + \theta''\phi\big) = 0, \tag{18}$$

The relevant boundary conditions are reduced to the form:

$$\begin{array}{l} f = f_w, f' = 1, \theta = 1, \phi = 1 \quad at\, \eta = 0, \\ f' = 0, \theta = 0, \phi = 0 \quad at\, \eta \to \infty. \end{array} \tag{19}$$

The dimensional physical parameters after simplification are defined as:

$$\begin{array}{l} \lambda = \frac{c}{a}, \beta = \lambda\left(\frac{a}{1-ct}\right), M = \frac{\sigma {B_0}^2}{\rho a}(1-\alpha t), EI = EI = \frac{E_0}{axB_0}(1-\alpha t), Nt = -\frac{k_1(T_w - T_\infty)}{T_r}, \\ Sc = \frac{\nu}{D_m}, Sc = \frac{\nu}{\alpha}, Rd = \frac{4T_\infty^3 \sigma^*}{3kK^*}. \end{array} \tag{20}$$

where Pr represents the Prandtl number, EI is the electric parameter, Rd represents the radiation parameter, λ is the unsteadiness parameter, M is the magnetic parameter, Nt is the thermophoresis parameter, Sc is Schmidt number and β is the Deborah number.

3. Physical Quantities of Interest

The physical quantities of interest for the governing Maxwell nanofluid flow problem are Skin friction C_f, local Nusselt number Nu_x, and local Sherwood number Sh_x, which are defined as:

$$C_f = \frac{Nt}{\rho U_w^2/2}, \; Nu_x = \frac{xq_w}{\kappa(T_w - T_\infty)}, \; Sh_x = \frac{xJ_w}{D_m(C_w - C_\infty)}, \tag{21}$$

where J_w, Nt and q_w are the mass flux, surface heat flux and wall shear stress, respectively. Substituting Equation (11) into Equation (21), the dimensionless form of these main design quantities are:

$$C_f = \frac{f''(0)}{\mathrm{Re}_{x^{1/2}}}, \; Nu_x = -(1 + \frac{4}{3}Rd)\theta'(0)\mathrm{Re}_{x^{1/2}}, \; Sh_x = -\phi'(0)\mathrm{Re}_{x^{1/2}}, \tag{22}$$

4. Solution by HAM

Lieo [40–42] worked for the first time on HAM (Homotopy analysis method). He used the idea of Homotopy from in topology and introduced HAM. When one of the functions is not clearly in another, then this is a homotopic function. Consider two continuous functions f_1, f_2 and two topological spaces X, Y. Wherever the two functions map from X to Y, f_1 is known as homotopic to f_2 if it produces continuous function

$$\psi : X \times [0, 1] \to Y. \tag{23}$$

Such that $\forall$, $x \in X$

$$\psi[x, 0] = f_1(x) \;\&\; \psi[x, 1] = f_2(x). \tag{24}$$

Then, the mapping is called homotopic. HAM is an alternative method and it is used to solve non-linear differential equation not including linearization and discretization. To solve Equations (16)–(18), the Homotopy Analysis Method (HAM) is used. HAM utilizes the suitable boundary condition in Equation (19) successfully. The given explanations exhibit the supplementary parameters $\hbar$ which control and normalize the convergence of this very solution.

The initial guesses are selected as follows

$$\widetilde{f}_0(\eta) = 1 + \widetilde{f}_w + e^{-\eta}, \; \widetilde{\theta}_0(\eta) = e^{-\eta}, \; \widetilde{\phi}_0(\eta) = e^{-\eta}. \tag{25}$$

The linear operators in use are L_φ, L_f and L_θ:

$$L_f(f) = f_{\eta\eta\eta} - f_\eta, \; L_\theta(\theta) = \theta_{\eta\eta} - \theta, \; L_\varphi(\phi) = \phi_{\eta\eta} - \phi, \tag{26}$$

which exhibit the following properties:

$$L_f(F_1 + F_2e^{-\eta} + F_3e^{\eta}) = 0,\ L_\theta(F_4e^{-\eta} + F_5e^{\eta}) = 0\ ,\ L_\phi(F_6e^{-\eta} + F_7e^{\eta}) = 0, \tag{27}$$

where $F_i (i = 1\text{–}7)$ are the constants in this wide-ranging solution. The subsequent non-linear operatives N_θ, N_ϕ and N_f are specified as:

$$\begin{aligned} N_f[\widetilde{f}(\eta;\zeta)] &= \tfrac{\partial^3\widetilde{f}(\eta;\zeta)}{\partial\eta^3} + \widetilde{f}(\eta;\zeta)\tfrac{\partial^2\widetilde{f}(\eta;\zeta)}{\partial\eta^2} - \left(\tfrac{\partial\widetilde{f}(\eta;\zeta)}{\partial\eta}\right)^2 - M\tfrac{\partial\widetilde{f}(\eta;\zeta)}{\partial\eta} - MEI, \\ -\lambda\left(\tfrac{\partial\widetilde{f}(\eta;\zeta)}{\partial\eta} + \tfrac{\eta}{2}\tfrac{\partial^2\widetilde{f}(\eta;\zeta)}{\partial\eta^2}\right) &- \beta\left(\begin{array}{c}\left(\tfrac{\partial\widetilde{f}(\eta;\zeta)}{\partial\eta}\right)^2\tfrac{\partial^3\widetilde{f}(\eta;\zeta)}{\partial\eta^3} - \\ 2\widetilde{f}(\eta;\zeta)\tfrac{\partial\widetilde{f}(\eta;\zeta)}{\partial\eta}\tfrac{\partial^3\widetilde{f}(\eta;\zeta)}{\partial\eta^3}\end{array}\right) \end{aligned} \tag{28}$$

$$\begin{aligned} &N_\theta\left[\widetilde{f}(\eta;\zeta),\widetilde{\theta}(\eta;\zeta)\right] = \left(1 + \tfrac{4}{3}Rd\right)\tfrac{\partial^2\widetilde{\theta}(\eta;\zeta)}{\partial\eta^2} - \\ &\Pr\left[\widetilde{f}(\eta;\zeta)\tfrac{\partial\widetilde{\theta}(\eta;\zeta)}{\partial\eta} - \tfrac{\partial\widetilde{f}(\eta;\zeta)}{\partial\eta}\widetilde{\theta}(\eta;\zeta) - \lambda\left(\widetilde{\theta}(\eta;\zeta) + \tfrac{\eta}{2}\tfrac{\partial\widetilde{\theta}(\eta;\zeta)}{\partial\eta}\right)\right] \\ &+A\tfrac{\partial\widetilde{f}(\eta;\zeta)}{\partial\eta} + B\widetilde{\theta}(\eta;\zeta), \end{aligned} \tag{29}$$

$$\begin{aligned} &N_\phi\left[\widetilde{f}(\eta;\zeta),\widetilde{\theta}(\eta;\zeta),\widetilde{\phi}(\eta;\zeta)\right] = \tfrac{\partial^2\widetilde{\phi}(\eta;\zeta)}{\partial\eta^2} + \\ &Sc\left[\widetilde{f}(\eta;\zeta)\tfrac{\partial\widetilde{\phi}(\eta;\zeta)}{\partial\eta} - \tfrac{\partial\widetilde{f}(\eta;\zeta)}{\partial\eta}\widetilde{\phi}(\eta;\zeta) - \lambda\left(3\widetilde{\phi}(\eta;\zeta) + \tfrac{\eta}{2}\tfrac{\partial\widetilde{\phi}(\eta;\zeta)}{\partial\eta}\right)\right] \\ &-Nt\left(\tfrac{\partial\widetilde{\theta}(\eta;\zeta)}{\partial\eta}\tfrac{\partial\widetilde{\phi}(\eta;\zeta)}{\partial\eta} + \tfrac{\partial^2\widetilde{\theta}(\eta;\zeta)}{\partial\eta^2}\widetilde{\phi}(\eta;\zeta)\right), \end{aligned} \tag{30}$$

The zero-order problems are

$$\begin{aligned} (1-\zeta)L_f\left[\widetilde{f}(\eta;\zeta) - \widetilde{f}_0(\eta)\right] &= \zeta\hbar_f N_f\left[\widetilde{f}(\eta;\zeta)\right], \\ (1-\zeta)L_\theta\left[\widetilde{\theta}(\eta;\zeta) - \widetilde{\theta}_0(\eta)\right] &= \zeta\hbar_\theta N_\theta\left[\widetilde{f}(\eta;\zeta),\widetilde{\theta}(\eta;\zeta)\right], \\ (1-\zeta)L_\phi[\widetilde{\phi}(\eta;\zeta) - \widetilde{\phi}_0(\eta)] &= \zeta\hbar_\phi N_\phi\left[\widetilde{f}(\eta;\zeta),\widetilde{\theta}(\eta;\zeta),\widetilde{\phi}(\eta;\zeta)\right]. \end{aligned} \tag{31}$$

The equivalent boundary conditions are:

$$\begin{aligned} &\widetilde{f}(\eta;\zeta)\Big|_{\eta=0} = \widetilde{f}_w,\ \tfrac{\partial\widetilde{f}(\eta;\zeta)}{\partial\eta}\Big|_{\eta=0} = 1,\ \tfrac{\partial\widetilde{f}(\eta;\zeta)}{\partial\eta}\Big|_{\eta\to\infty} = 0, \\ &\widetilde{\theta}(\eta;\zeta)\Big|_{\eta=0} = 1,\ \widetilde{\theta}(\eta;\zeta)\Big|_{\eta\to\infty} = 0,\ \widetilde{\phi}(\eta;\zeta)\big|_{\eta=0} = 1,\ \widetilde{\phi}(\eta;\zeta)\big|_{\eta\to\infty} = 0 \end{aligned} \tag{32}$$

where $\zeta \in [0,1]$ is the imbedding parameter, and $\hbar_f$, $\hbar_\theta$ and $\hbar_\phi$ are used to control the convergence of the solution. When $\zeta = 0$ and $\zeta = 1$, we have:

$$\widetilde{f}(\eta;1) = \widetilde{f}(\eta),\ \widetilde{\theta}(\eta;1) = \widetilde{\theta}(\eta) \text{ and } \widetilde{\phi}(\eta;1) = \widetilde{\phi}(\eta), \tag{33}$$

Expanding $\widetilde{f}(\eta;\zeta)$, $\widetilde{\theta}(\eta;\zeta)$ and $\widetilde{\phi}(\eta;\zeta)$ in Taylor's series about $\zeta = 0$,

$$\begin{aligned} \widetilde{f}(\eta;\zeta) &= \widetilde{f}_0(\eta) + \sum_{m=1}^{\infty}\widetilde{f}_m(\eta)\zeta^m, \\ \widetilde{\theta}(\eta;\zeta) &= \widetilde{\theta}_0(\eta) + \sum_{m=1}^{\infty}\widetilde{\theta}_m(\eta)\zeta^m, \\ \widetilde{\phi}(\eta;\zeta) &= \widetilde{\phi}_0(\eta) + \sum_{m=1}^{\infty}\widetilde{\phi}_m(\eta)\zeta^m. \end{aligned} \tag{34}$$

where

$$\widetilde{f}_m(\eta) = \frac{1}{m!}\frac{\partial \widetilde{f}(\eta;\zeta)}{\partial \eta}\bigg|_{\zeta=0}, \ \widetilde{\theta}_m(\eta) = \frac{1}{m!}\frac{\partial \widetilde{\theta}(\eta;\zeta)}{\partial \eta}\bigg|_{\zeta=0} \text{ and } \widetilde{\phi}_m(\eta) = \frac{1}{m!}\frac{\partial \widetilde{\phi}(\eta;\zeta)}{\partial \eta}\bigg|_{\zeta=0}. \tag{35}$$

The secondary constraints $\hbar_\varphi$, $\hbar_\theta$ and $\hbar_f$ are taken in such form that the sequences in Equation (34) converge at $\zeta = 1$. Switching $\zeta = 1$ in Equation (35), we obtain:

$$\begin{aligned} \widetilde{f}(\eta) &= \widetilde{f}_0(\eta) + \sum_{m=1}^{\infty} \widetilde{f}_m(\eta), \\ \widetilde{\theta}(\eta) &= \widetilde{\theta}_0(\eta) + \sum_{m=1}^{\infty} \widetilde{\theta}_m(\eta), \\ \widetilde{\phi}(\eta) &= \widetilde{\phi}_0(\eta) + \sum_{m=1}^{\infty} \widetilde{\phi}_m(\eta). \end{aligned} \tag{36}$$

The m^{th} -order problem, fulfills the following:

$$\begin{aligned} L_f\left[\widetilde{f}_m(\eta) - \chi_m \widetilde{f}_{m-1}(\eta)\right] &= \hbar_f R_m^f(\eta), \\ L_\theta\left[\widetilde{\theta}_m(\eta) - \chi_m \widetilde{\theta}_{m-1}(\eta)\right] &= \hbar_\theta R_m^\theta(\eta), \\ L_\varphi\left[\widetilde{\phi}_m(\eta) - \chi_m \widetilde{\phi}_{m-1}(\eta)\right] &= \hbar_\varphi R_m^\varphi(\eta). \end{aligned} \tag{37}$$

The consistent boundary conditions are:

$$\begin{aligned} f_m(0) = f'_m(0) = \theta_m(0) = \phi_m(0) = 0 \\ f'_m(\infty) = \theta_m(\infty) = \phi_m(\infty) = 0 \end{aligned} \tag{38}$$

where

$$\begin{aligned} R_m^f(\eta) &= f'''_{m-1} + \sum_{k=0}^{m-1} f_{m-1-k} f''_k - \sum_{k=0}^{m-1} f'_{m-1-k} f'_k \\ &-\lambda\left[f'_{m-1} + \tfrac{\eta}{2} f''_{m-1}\right] - \beta\left[\sum_{k=0}^{m-1} f'_{m-1-k} \sum_{l=0}^{k} f'_{k-l} f'''_l - 2\sum_{k=0}^{m-1} f_{m-1-k} \sum_{l=0}^{k} f'_{k-l} f'''_l\right] \\ &-M f'_{m-1} - MEI, \end{aligned} \tag{39}$$

$$\begin{aligned} R_m^\theta(\eta) &= \left(1 + \tfrac{4}{3}Rd\right)\theta''_{m-1} + \\ &\Pr\left[\sum_{k=0}^{m-1} f_{m-1-k}\theta'_k - \sum_{k=0}^{m-1} \theta_{m-1-k} f'_k - \lambda\left(\theta_{m-1} + \tfrac{\eta}{2}\theta'_{m-1}\right)\right] \\ &+A f'_{m-1} + B\theta_{m-1}, \end{aligned} \tag{40}$$

$$\begin{aligned} R_m^\varphi(\eta) &= \phi'_{m-1} + Sc\left[\sum_{k=0}^{m-1} f_{m-1-k}\phi'_j - \sum_{k=0}^{m-1} f'_{m-1-k}\varphi_k - \lambda\left(3\phi_{m-1} + \tfrac{\eta}{2}\phi'_{m-1}\right)\right] \\ &-Nt\left[\sum_{k=0}^{m-1} \theta'_{m-1-k}\phi'_j + \sum_{k=0}^{m-1} \theta''_{m-1-k}\phi_j\right], \end{aligned} \tag{41}$$

where

$$\chi_m = \begin{cases} 0, & \text{if } \zeta \le 1 \\ 1, & \text{if } \zeta > 1 \end{cases} \tag{42}$$

5. Discussion

5.1. Graphical Discussion

The purpose of this segment is to discuss the physical properties of different embedding parameters in the stated flow problem on the velocity profile, temperature profile and concentration profile, which are illustrated in Figures 2–13. Figure 2 shows velocity variations due to unsteady parameter. Increasing the value of unsteady factor results in decrease of the velocity of the fluid,

which is understandable because velocity remains faster in steady and stretching flow. Figure 3 shows the effect of the unsteady parameter on concentration profile. It is obvious from the graph that increasing the unsteady parameter λ decreases the concentration. The influence of λ is normal because, due to stretching sheet and steady flow, both the concentration and temperature increases, while increasing the unsteady parameter cause the reverse effect. The concentration variation starts from $\eta = 4$. Figure 4 shows the variation of temperature due to unsteady parameter. The effect of unsteady factor on temperature is similar to the concentration of the fluid. Increasing the value of λ decreases temperature profile of the nanofluid. This shows that cooling ratio will be faster as compared to steady flow. It is expected that, in unsteady flow, the spaces between the molecules increases, thus concentrations and the temperature profile decrease. Thus, for practical purposes, these factors are highlighted here. Designing any apparatus, the unsteady factor should be well considered.

Figure 5 shows the magnetic field influence on the velocity of the nanofluid. Increasing the value of M results in reduction of the strength of the velocity of the fluid because the magnetic field produces a Lorentz force that is against the flow of the fluid. The magnetic field is applied perpendicular to the flow and produces maximum Lorentz force. It reduces the thickness of the momentum boundary layer as well. The thermal boundary layer increases with increasing values of magnetic field. Figure 6 depicts the effect of Deborah number on the velocity of the fluid. Increasing the value of Deborah number decreases the velocity of the fluid. The momentum boundary layer thickness decreases with increasing of the Deborah number. Actually, the influence of the Deborah number reverses when Newtonian fluids are used: the thickness of the layer increases by increases of the Maxwell factor.

Figure 7 shows the impact of radiation strength on the temperature of the nanofluid. Increasing the value of the radiations increases the temperature of the Nanofluid. The thickness of the thermal boundary layer also increases. One can control the temperature of the fluid from thermal radiations because the temperature is very sensitive to thermal radiations, which means that the heat flux at the surface will be greater. The thermal boundary layer thickness increases with an increase in the value of the thermal boundary layer. Figure 8 shows the Prandtl number effect on the temperature of the Nanofluid. Increasing the Pr number reduces the thermal boundary layer thickness and temperature of the Nanofluid. The reason behind this is that Pr is a ratio of momentum diffusivity to thermal diffusivity. When thermal diffusivity decreases, automatically Pr number increases and the temperature of the fluid decreases. In other words, Pr and temperature have an inverse relation. Prandtl number controls the relative thickening of the momentum boundary layer and thermal boundary layer. One can easily control or predict the rate of flow and temperature knowing the value of Prandtl number. Figure 9 illustrates space dependent parameter for the Nanofluid. Increasing the value of the space dependent factor A increases the temperature of the Nanofluid. Similarly, Figure 10 shows the case of temperature dependent coefficient. It also increases temperature by increasing the value of B. With the increases of parameters A and B, the thermal layer of the boundary produces energy, which raises the temperature profile. Decreasing the values of A and B decreases the thermal boundary layer thickness and result in decrease of temperature.

Figure 11 depicts the consequences of thermophoretic parameter on the concentration of the fluid. The effect of thermophoresis parameter on the concentration profile is monotonic, which means that increase in thermophoresis parameter is sensitive to concentration profile. Increasing the value of the thermophoretic parameter decreases the concentration of the fluid. The reason is that the values of thermophoretic parameter are positive and the fluid flow is directed from hot toward the cold surface. Thus, it is concluded that imposition of thermophoretic parameter on the fluid flow enhances the thickness of the thermal layer. Figure 12 is the effect of Sc on $\phi(\eta)$. Increasing the value of Sc decreases the concentration of the fluid. Sc is Schmidt number. Actually, Sc depends on Brownian diffusivity. Increasing Sc leads to the lower value of the concentration field because decreases in Brownian diffusivity have the inverse relation with Sc. Figure 13 depicts the influence of electric field on the velocity of the fluid. The velocity of the fluid increases with increase value of the electric field, but the combine effect of the electric and magnetic field produces Lorentz forces which result in

decreasing the $f(\eta)$ of the fluid. The momentum boundary layer thickness increases with the increase in the value of the electric field.

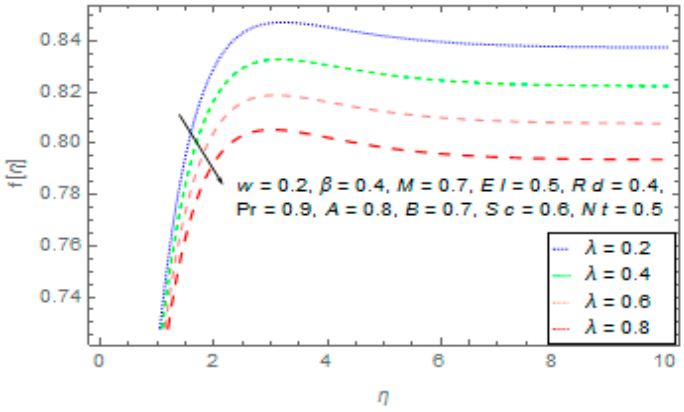

Figure 2. Influence of λ on velocity profile.

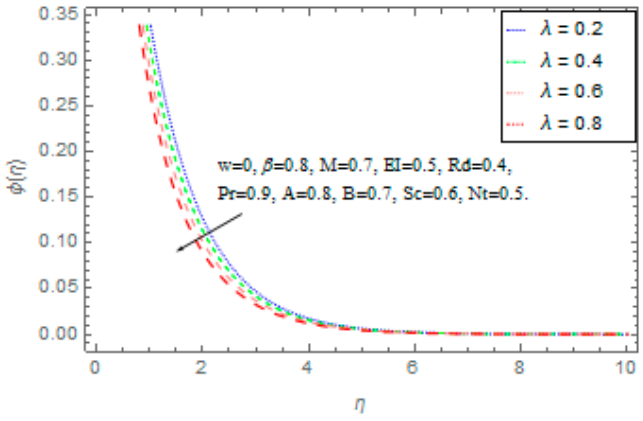

Figure 3. Influence of λ on concentration $\phi(\eta)$.

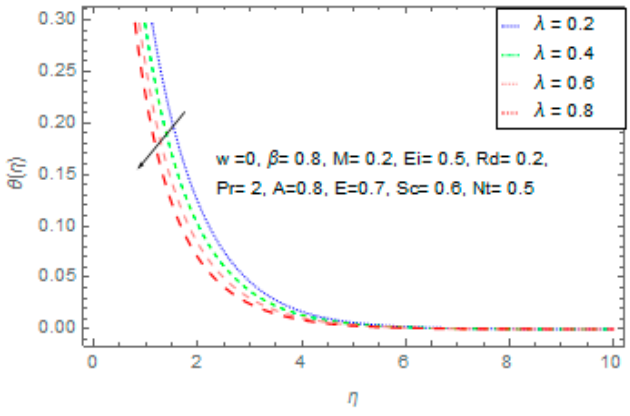

Figure 4. Influence of λ on $\theta(\eta)$.

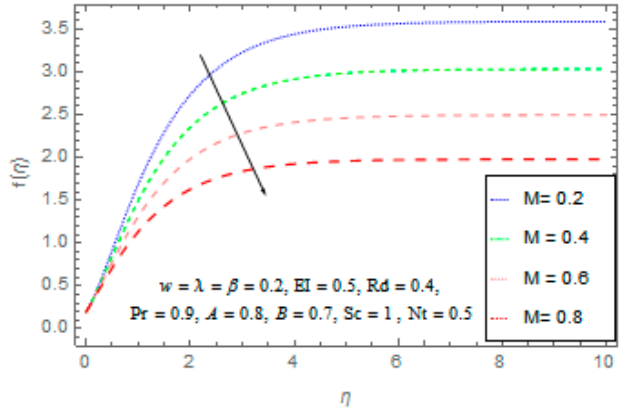

Figure 5. Influence of M on velocity Profile.

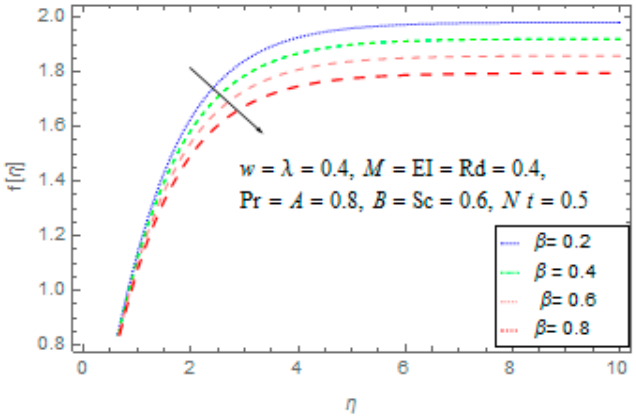

Figure 6. Influence of β on $f(\eta)$.

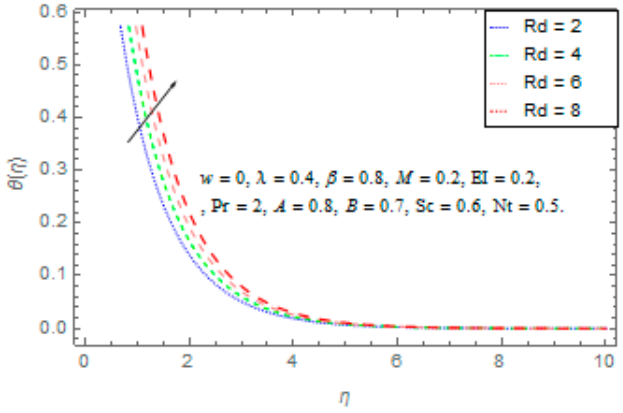

Figure 7. Influence of Rd on temperature profile.

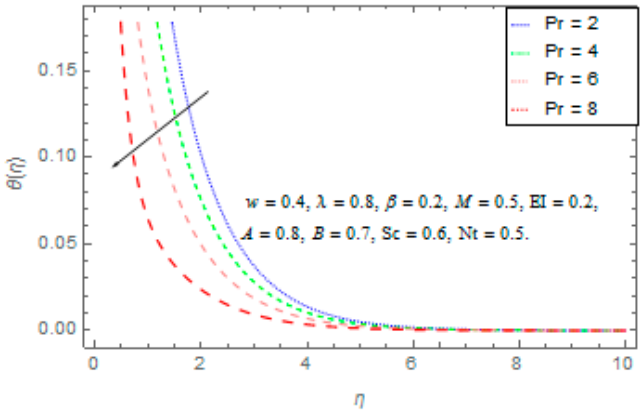

Figure 8. Influence of Pr on $\theta(\eta)$ of the fluid.

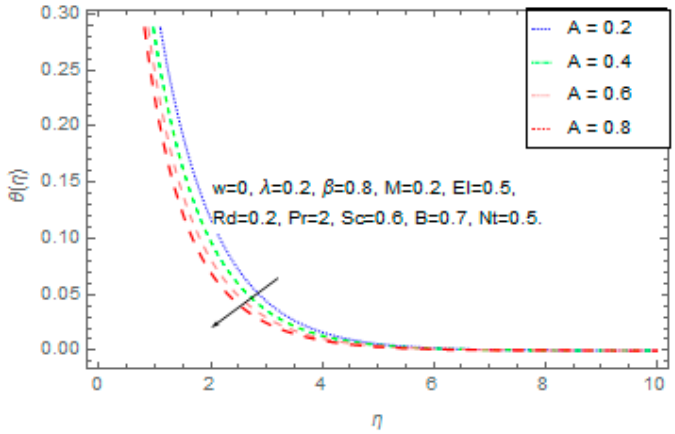

Figure 9. Influence of A on $\theta(\eta)$ Profile.

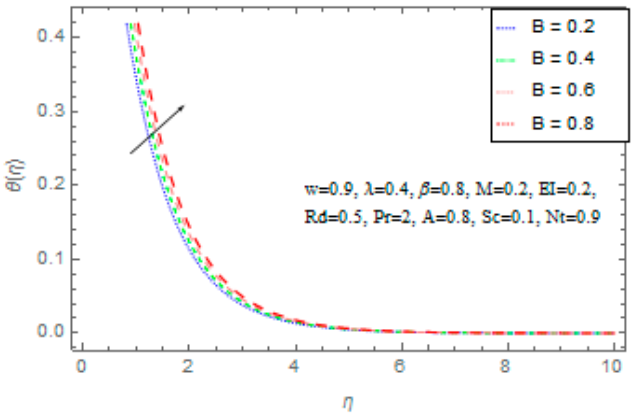

Figure 10. Influence of B on $\theta(\eta)$ Profile.

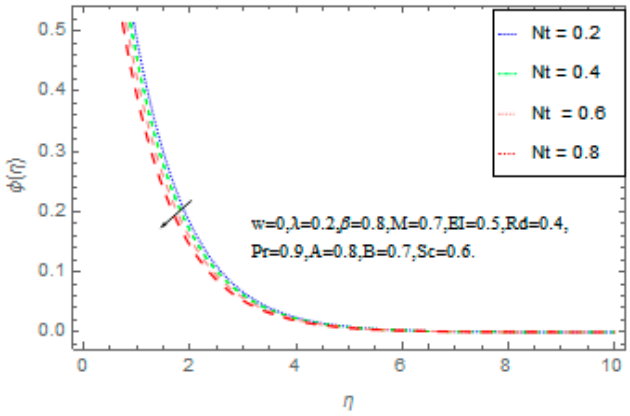

Figure 11. Influence of Nt on $\phi(\eta)$ Profile.

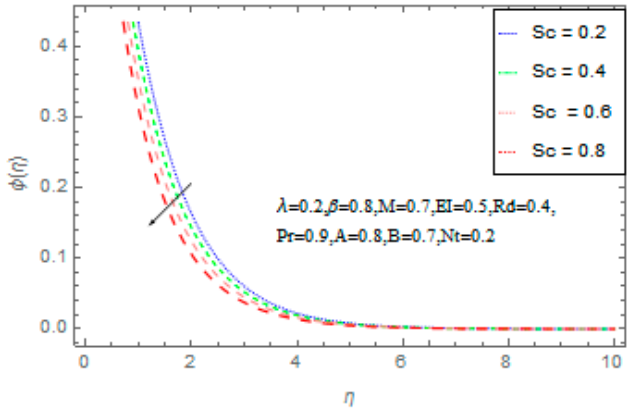

Figure 12. Influence of Sc on $\phi(\eta)$ of the fluid.

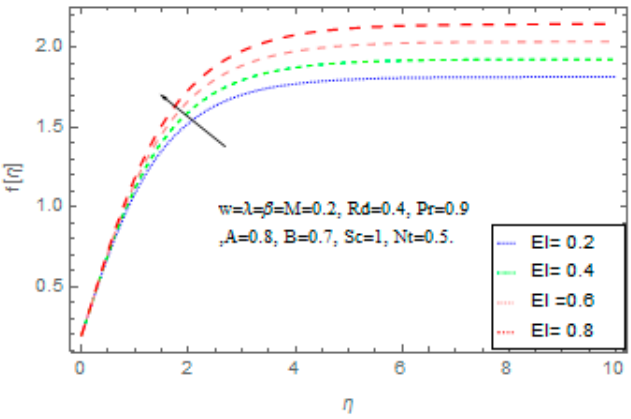

Figure 13. Influence of EI on velocity profile.

5.2. Discussion of Tables

Tables 1–3 depict the influence of skin friction, Sherwood number and Nusselt number due to altered parameters. The effects of M, EI, λ and β on skin friction are shown in Table 1. It is observed that increasing rate of M, EI, λ and β decreases the Skin-friction coefficient. The effects of Rd, λ, A and B on the Nusselt number are shown in Table 2. It is observed that increasing rate of radiation strength reduces the Nusselt number, while the unsteady parameter λ increases the Nusselt number. It is perceived that increase in the value of space dependent parameter and temperature dependent parameter reduces the heat flux.

The effects of Sc, Nt and λ on the Sherwood Number are shown in Table 3. In Table 3, it is noticed that local Sherwood number values increases due to increase in thermophoretic parameter. Increasing the Schmidt number decreases the Sherwood number, while increasing unsteady parameter decreases the Sherwood number.

The comparison with previous results [3] have been done. We have found good match in the behavior of all the parameters discussed in our problem. The variations in the tables have little differences, which is due to different fluids, as one is a Newtonian fluid and the other is a Maxwell fluid, but the actual trend matches.

Table 1. Variation in Skin-Friction Coefficient of various parameters where $\omega = Rd = \Pr = Nt = Nb = Sc = \delta = 0.1$.

M	EI	λ	β	C_f Reddy et al. [3] Results	C_f Present Results
0.1				−1.5158744	−1.74875
0.5				−1.6666449	−1.91320
1.0				−1.8346139	−1.91302
1.5				−1.9860796	−2.30777
0.5				−1.4519989	−2.11320
	0.1			−1.5557482	−1.74875
	0.5			−1.6666449	−1.77085
	1.0			−1.7845786	−1.79849
	1.5			−1.3363316	−1.82613
	0.5			−1.3257839	−1.77085
		0.1		−1.3704027	−1.62822
		0.5		−1.4023647	−1.74875
		1.0		−1.1278748	−1.89622
		1.5		−1.2578397	−2.04021
		0.5		−1.6594641	−1.74875
			0.1	−1.7868723	−1.15896
			0.5	−1.2867381	−1.62822
			1.0	−1.3188963	−2.26780
			1.5	−1.3748052	−2.98208

Table 2. Variation in the Nusselt number of dissimilar parameters $\omega = M = EI = \Pr = Nt = Sc = \beta = 0.1$.

Rd	λ	A	B	Nu_x Reddy et al. [3] Results	Nu_x Presents Results
0.1				1.0954583	0.418189
0.5				1.0769383	0.365972
1.0				1.0581713	0.325005
1.5				1.0427808	0.303409
0.5				0.9558400	0.365972
	0.1			1.0142059	0.384688
	0.5			1.0769383	0.429300
	1.0			1.1440810	0.484446
	1.5			1.0638213	0.538907
	0.5			0.8488358	0.429300
		0.1		0.7413729	0.712750
		0.5		0.5802159	0.619018
		1.0		0.9273635	0.501853
		1.5		0.8488358	0.384688
		0.5		0.7619111	0.619018

Table 2. *Cont.*

Rd	λ	*A*	*B*	Nu_x Reddy et al. [3] Results	Nu_x Presents Results
			0.1	0.6631123	0.810743
			0.5	1.0967356	0.712750
			1.0	0.9541261	0.587160
			1.5	0.7670185	0.458056

Table 3. Variation in the Sherwood Number of dissimilar parameters $\omega = M = EI = Rd = \Pr = \beta = 0.1$.

Sc	*Nt*	λ	Sh_x Reddy et al. [3] Results	Sh_x Present Results
0.1			1.4353078	1.955299
0.5			1.4044462	1.660820
1.0			1.3724033	1.407640
1.5			1.3455601	1.643610
0.5			1.2787791	1.660820
	0.1		1.3398008	0.836947
	0.5		1.4044462	0.955299
	1.0		1.4731732	1.107160
	1.5		1.0989064	1.263380
	0.5		1.2599294	0.955299
		0.1	1.3403629	0.814646
		0.5	1.4609154	0.844357
		1.0	1.2046987	0.781225
		1.5	1.2599294	0.717796
		0.5	1.3199523	0.844357

6. Conclusions

The influences of electric field, magnetic field and thermal radiation on Maxwell nanofluid flow are studied. The schematic diagram is shown in Figure 1. The flow has been taken along y-axis where magnetic and electric fields are supplied. The modeled equations have been solved through the analytical homotopy analysis method (HAM). The influences have been shown graphically. The variation of Skin friction, Nusselt number and Sherwood number is discussed. Further, for a clearer picture, the physical parameters, namely, unsteady parameter λ, Maxwell parameter β, magnetic parameter M, radiation parameter Rd, electric parameter E, thermophoresis parameter Nt, Schmidt number Sc, Prandtl number Pr, space dependent coefficient (A) and temperature dependent coefficient (B), acting on concentration $\phi(\eta)$, velocity $f(\eta)$ and temperature $\theta(\eta)$, are analyzed and studied in detail. The main conclusions are as follows.

- The magnetic parameter M, has the reverse effect on velocity, which means that increasing the magnetic field value results in a decrease of the velocity of the nanofluid. This is due to the Lorentz forces, which are against the flow of the fluid.
- Increasing Schmidt number decreases the concentration profile $\phi(\eta)$, which is consistent with previous results.
- The unsteady parameter λ shows decreasing behavior in velocity profile, concentration profile $\phi(\eta)$ and temperature profile $\theta(\eta)$ of the fluid.
- The effect of radiation Rd on temperature matches common observations. It increases the temperature of the fluid. It is also observed that high radiations cause a high temperature.
- Increasing the value of the thermophoretic parameter Nt, decreases the concentration $\phi(\eta)$ of the nanofluid.

- The velocity of the nanofluid increases with increasing value of the electric field, but the combined effect of the electric and magnetic field produces Lorentz forces, which result in a decrease of the velocity of the fluid.
- It is noted that increasing the Deborah number decreases the velocity of the Nanofluid.

Author Contributions: H.K. and Z.S. modeled the problem; H.K. and M.H. wrote the paper; M.H., S.I. and S.M. made the corrections and arranged the paper; and W.K. and Z.S. solved the problem.

Conflicts of Interest: The authors declare no conflict of interest.

References

1. Alfven, H. Existence of electromagnetic-hydrodynamic waves. *Nature* **1942**, *150*, 405–406. [CrossRef]
2. Mahanthesh, B.; Gireesha, B.J.; Reddy, G.R.S. Unsteady three-dimensional MHD flow of a nano Eyring-Powell fluid past a convectively heated stretching sheet in the presence of thermal radiation, viscous dissipation and Joule heating. *J. Assoc. Arab Univ. Basic Appl. Sci.* **2017**, *23*, 75–84. [CrossRef]
3. Reddy, P.S.; Chamka, A.J. Soret and Dufour Effects on Unsteady MHD Heat and Mass Transfer from a Permeable Stretching Sheet with Thermophoresis and Non-Uniform Heat Generation/Absorption. *J. Appl. Fluid Mech.* **2016**, *9*, 2443–2455. [CrossRef]
4. Choi, S.U.S. Nanofluids from vision to reality through research. *J. Heat Transf.* **2009**, *131*, 033106. [CrossRef]
5. Yu, W.; France, D.M.; Routbort, J.L.; Choi, S.U.S. Review and comparison of nanofluid thermal conductivity and heat transfer enhancements. *Heat Transf. Eng.* **2008**, *29*, 432–460. [CrossRef]
6. Tyler, T.; Shenderova, O.; Cunningham, G.; Walsh, J.; Drobnik, J.; McGuire, G. Thermal transport properties of diamond based nanofluids and nanocomposites. *Diam. Relat. Mater.* **2006**, *15*, 2078–2081. [CrossRef]
7. Das, S.K.; Choi, S.U.S.; Patel, H.E. Heat transfer in nanofluids—A review. *Heat Transf. Eng.* **2006**, *27*, 3–19. [CrossRef]
8. Liu, M.S.; Lin, M.C.-C.; Huang, I.-T.; Wang, C.-C. Enhancement of thermal conductivity with carbon nanotube for nanofluids. *Int. Commun. Heat Mass Transf.* **2005**, *32*, 1202–1210. [CrossRef]
9. Nicolas, G.G.; Antonio, R.; Antonio, G. Electric field induced fluid flow on microelectrodes: the effect of illumination. *J. Phys. D Appl. Phys.* **2000**, *33*, L13–L17.
10. Velkoff, H.R.; Godfrey, R. Low-Velocity Heat Transfer to a Flat Plate in The Presence of a Corona Discharge in Air. *J. Heat Transf.* **1979**, *101*, 157–163. [CrossRef]
11. Yan, Y.Y.; Zhang, H.B.; Hull, J.B. Numerical Modeling of Electrohydrodynamic (EHD) Effect on Natural Convection in an Enclosure. *Numer. Heat Transf. Part A Appl.* **2004**, *46*, 453–471. [CrossRef]
12. Hsu, J.P.; Kao, C.Y.; Tseng, S.; Chen, C.J. Electrokinetic transport in unsteady flow through peristaltic microchannel. *J. Colloid Interface Sci.* **2002**, *248*, 176–184. [CrossRef] [PubMed]
13. Monajjemi, R.E.; Nasr, E.M. Influence of the uniform electric field on viscosity of magnetic nanofluid. *J. Appl. Phys.* **2012**, *112*, 094903. [CrossRef]
14. Plumb, O.A.; Huenfeld, J.S.; Eschbach, E.J. The effect of cross flow and radiation on natural convection from vertical heated surfaces in saturated porous media. In Proceedings of the AIAA 16th Thermophysics Conference, Palo Alto, CA, USA, 23–25 June 1981.
15. Grubka, L.G.; Bobba, K.M. Heat transfer characteristics of a continuous stretching surface with variable temperature. *J. Heat Transf.* **2015**, *107*, 248–250. [CrossRef]
16. Watson, G.H.; Lee, A.L. Thermal radiation model for solid rocket booster plumes. *J. Spacecr. Rockets* **1977**, *14*, 641–647. [CrossRef]
17. Rajesh, V.; Anwar, B.; Mallesh, M.P. Transint nanofluid flow and heat transfer from a moving vertical cylinder in the presence of thermal radiation. *J. Nanomater. Nanoeng. Nanosyst.* **2016**, *230*, 3–10.
18. Yang, G.; Ebadian, M.A. Radiation convection in a thermally developing duct flow of noncircular cross section. *J. Thermophys. Heat Transf.* **1999**, *5*, 224–231. [CrossRef]
19. Nansour, M.A.; El Shear, N.A. Radiative effects on magnetohydrodynamic Natural Convection flows saturated in porous media. *J. Magn. Magn. Mater.* **2001**, *237*, 327–341. [CrossRef]
20. Sheikholeslamia, M.; Ganji, D.D.; Javed, Y.M.; Ellahi, R. Effect of thermal radiation on magnetohydrodynamics nanofluid flow and heat transfer by means of two phase model. *J. Magn. Magn. Mater.* **2015**, *374*, 36–43. [CrossRef]

21. Sheikholeslamia, M.; Jalili, P. Magnetic field effect on nanofluid flow between two circular cylinders using AGM. *Alex. Eng. J.* **2017**. [CrossRef]
22. Khanafer, K.; Vafai, K.; Lightstone, M. Buoyancy-driven heat transfer enhancement utilizing nanofluids. *Int. J. Heat Mass Transf.* **2003**, *46*, 3639–3653. [CrossRef]
23. Sheikholeslami, M.; Gorj, B.M.; Ganji, D.D.; Soheil, S. Natural convection heat transfer in a nanofluidfilled inclined L-shaped enclosure. *IJST Trans. Mech. Eng.* **2014**, *38*, 217–226.
24. Safia, A.; Nadeem, S. Consequence of nanofluid on peristaltic transport of a hyperbolic tangentfluid model in the occurrence of apt (tending) magnetic field. *J. Magn. Magn. Mater.* **2014**, *358–359*, 183–191.
25. Safia, A.; Nadeem, S.; Anwar, H. Effects of heat and mass transfer on peristaltic flow of a Bingham fluid in the presence of inclined magnetic field and channel with different wave forms. *J. Magn. Magn. Mater.* **2014**, *362*, 184–192.
26. Sheikholeslami, M.; Gorji, B.M.; Ganji, D.D. Natural convection in a nanofluidfilled concentric annulus between an outer square cylinder and an inner elliptic cylinder. *Sci. Iran.* **2013**, *20*, 1241–1253.
27. Safia, A.; Nadeem, S.; Hanif, M. Numerical and analytical treatment on peristalticflow of Williamsonfluid in the occurrence of induced magnetic field. *J. Magn. Magn. Mater.* **2013**, *346*, 142–151.
28. Fetecau, C.; Corina, F. Starting solutions for the motion of a second grade fluid due to longitudinal and torsional oscillations of a circular cylinder. *Int. J. Eng. Sci.* **2006**, *44*, 788–796. [CrossRef]
29. Frank, M.; Drikakis, D. Solid-like heat transfer in confined liquids. *Microfluid. Nanofluid.* **2017**, *21*, 148. [CrossRef]
30. Frank, M.; Drikakis, D.; Asproulis, N. Thermal Conductivity of Nanofluid in Nanochannels. *Microfluid. Nanofluid.* **2015**, *19*, 1011–1017. [CrossRef]
31. Papanikolaou, M.; Frank, M.; Drikakis, D. Nanoflow over a fractal surface. *Phys. Fluids* **2016**, *28*, 082001. [CrossRef]
32. Sakiadis, B.C. Boundary layer behavior on continuous solid surfaces. *AIChE J.* **1961**, *7*, 26–28. [CrossRef]
33. Crane, L.J. Flow past a stretching sheet. *Z. Angew. Math. Phys.* **1970**, *21*, 645–647. [CrossRef]
34. Gupta, P.S.; Gupta, A.S. Heat and mass transfer on a stretching sheet with suction or blowing. *Can. J. Chem. Eng.* **1977**, *55*, 744–746. [CrossRef]
35. Takahashi, N.; Koseki, H.; Hirano, T. Temporal and spatial characteristics of radiation from large pool fires Bull. *Jpn. Assoc. Fire Sci. Eng.* **1999**, *49*, 27–33.
36. Wang, C.Y. Liquid film on an unsteady stretching surface. *Q. Appl. Math.* **1990**, *48*, 601–610. [CrossRef]
37. Elbashbeshy, E.M.A.; Bazid, M.A.A. Heat transfer over an unsteady stretching surface. *Heat Mass Transf.* **2004**, *41*, 1–4. [CrossRef]
38. Chamkha, A.J.; Ahmed, S.E. Similarity Solution for Unsteady MHD Flow Near a Stagnation Point of a Three Dimensional Porous Body with Heat and Mass Transfer, Heat Generation/Absorption and Chemical Reaction. *J. Appl. Fluid Mech.* **2011**, *4*, 87–94.
39. Molla, M.M.; Saha, S.C.; Hossain, M.A. Radiation effect on free convection laminar flow along a vertical flat plate with stream wise sinusoidal surface temperature. *Math. Comput. Model.* **2011**, *53*, 1310–1319. [CrossRef]
40. Liao, S.J. On the Analytic Solution of Magnetohydrodynamic Flows of Non-Newtonian Fluids over a Stretching Sheet. *J. Fluid Mech.* **2003**, *488*, 189–212. [CrossRef]
41. Liao, S.J. An Analytic Solution of Unsteady Boundary Layer Flows Caused by Impulsively Stretching Plate. *Commun. Nonlinear Sci. Numer. Simul.* **2006**, *11*, 326–339. [CrossRef]
42. Liao, S.J. On Homotopy Analysis Method for Nonlinear Problems. *Appl. Math. Comput.* **2004**, *147*, 499–513. [CrossRef]
43. Asproulis, N.; Kalweit, M.; Drikakis, D. A Hybrid Molecular Continuum Method using Point Wise Coupling. *Adv. Eng. Softw.* **2012**, *46*, 85–92. [CrossRef]
44. Kalweit, M.; Drikakis, D. Coupling strategies for hybrid molecular-continuum simulationmethods. *J. Mech. Eng. Sci.* **2008**, *222*, 797–806. [CrossRef]
45. Kalweit, M. Multiscale Methods for Micro/Nano Flows and Materials. *J. Comput. Theor. Nanosci.* **2008**, *5*, 1923–1938. [CrossRef]